Supporting information for

Ultralong cycling and wide temperature lithium metal batteries enabled by solid polymer electrolytes interpenetrated with poly(liquid crystal) network

Meng Yao[ab], Haitao Zhang[*ab], Kun Dong[a], Bosen Li[a], Chunxian Xing[a], Manyu Dang[c], Suojiang Zhang[*ab]

[a] Beijing Key Laboratory of Ionic Liquids Clean Process, Institute of Process Engineering, Chinese Academy of Sciences, Beijing, 100190, China

[b] School of Chemical Engineering, University of Chinese Academy of Sciences, Beijing, 100049, China

[c] Department of Electronic and Electrical, University College London, London, England

E-mail address: htzhang@ipe.ac.cn; sjzhang@ipe.ac.cn

Section 1

The ionic conductivities of SPES were tested on an electrochemical working station via alternating-current (AC) impedance analysis employing stainless steel (SS)/SPE/SS from 0.1 Hz to 10 kHz. The testing temperatures were in the range from 20 to 80 °C with a step size of 5 °C min^{-1}, and σ of SPE was calculated by electrochemical impedance spectra (EIS) using the equation:

$$\sigma = \frac{L}{S \cdot R_b} \tag{1}$$

Where R_b is the bulk resistance; L is the thickness; S is surface area of SPEs. The electrical conductivity of the solid electrolyte is calculated using the equation:

$$\Upsilon = \frac{I_S L}{US} \tag{2}$$

Activation energy E_a can be calculated according to the Vogel−Tammann−Fulcher (VTF) equation:

$$\sigma = AT^{-0.5} e^{\frac{-E_a}{R(T-T0)}} \tag{3}$$

The value of prefactor A is related to the effective charge carrier concentration. T_o means glass transition temperature (T_g). To test the electrochemical stability of the SPE, the LSV (linear sweep voltammetry) was investigated employing SS/SPE/Li under 1 mV s^{-1} scan rate from 2 to 6 V. t_{Li+} of SPE was measured by CHI604A with DC polarization and AC impedance employing a symmetric cell of Li/SPE/Li. The t^+ can be calculated according to the equation[1]:

$$t_{Li+} = \frac{I_S(\Delta V - I_0 R_{to})}{I_0(\Delta V - I_s R_{ts})} \quad (3)$$

Where I_0, I_s are the initial and steady current through the Li/SPE/Li cell, which were measured by DC polarization with a voltage (ΔV = 20 mV). R_{to} and R_{ts} are the initial and steady resistances between the SPE and Li metal electrode which were obtained by AC impedance in the frequency between 0.1 Hz and 10 kHz.

To further explore the compatibility of SPE with Li, the lithium striping/plating experiments employing the same cell was conducted in a LAND CT2001A battery test system at room temperature with the current density of 0.1 mA cm^{-1} (the sum of the charge and discharge times was 2 h).

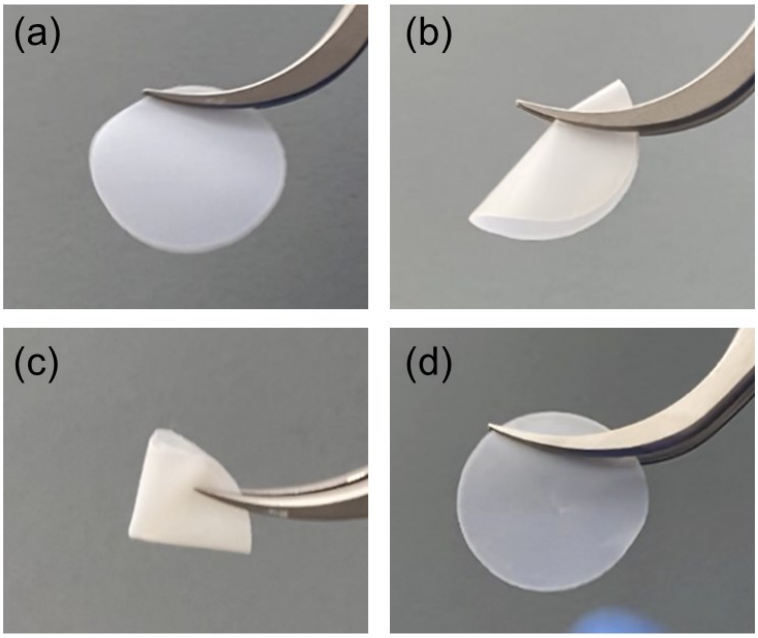

Fig. S1 Photographs of a) P-PLC-IL; b-c) folded and scrunched P-PLC-IL; and d) After being folded and scrunched , no damage on the P-PLC-IL is observed.

Fig. S2 Thickness of the porous P-PLC-IL SPE (60 μm).

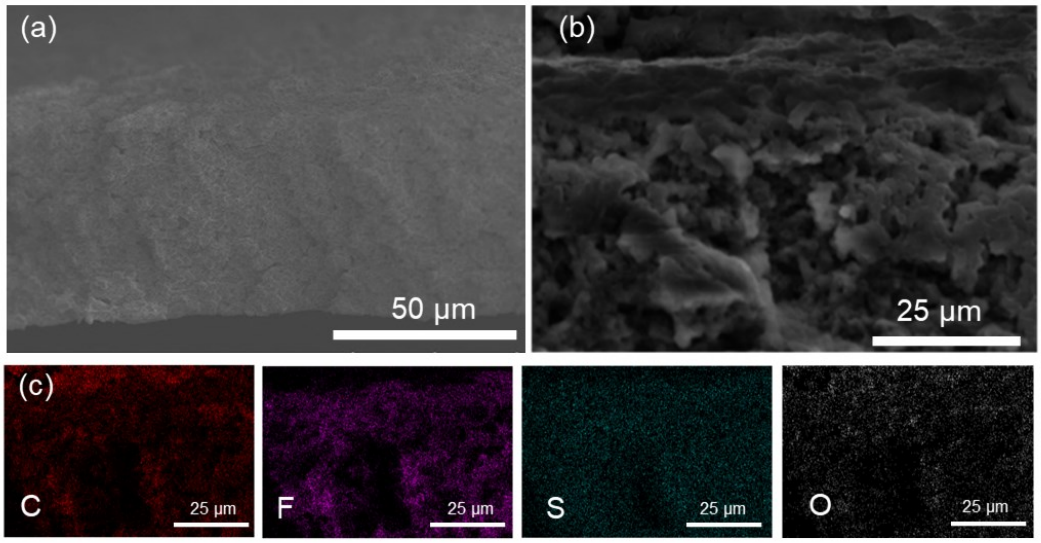

Fig. S3 a, b) SEM images of the cross section of SPE; c) EDS mapping of the cross section of SPE

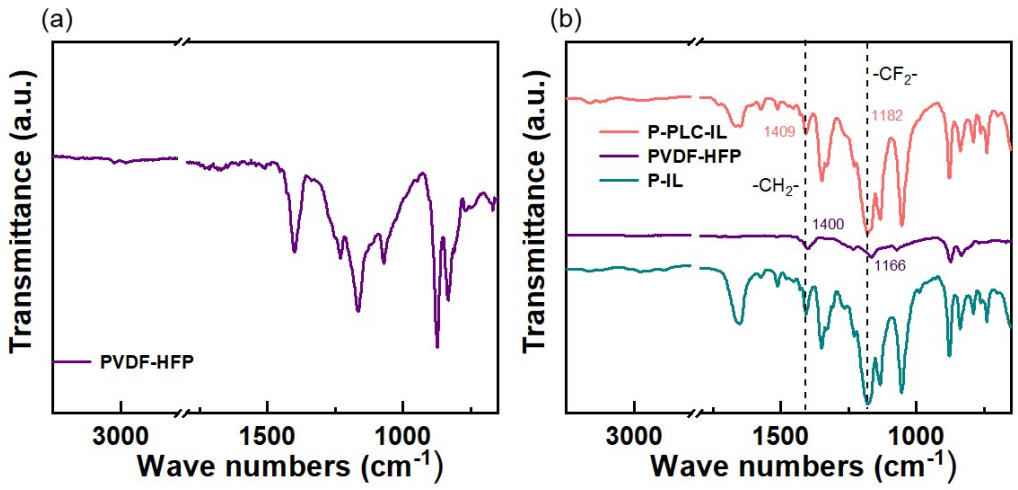

Fig. S4 a) FTIR spectrum of pristine PVDF-HFP; b) FTIR spectra of P-PLC-IL and P-IL SPEs and PVDF-HFP

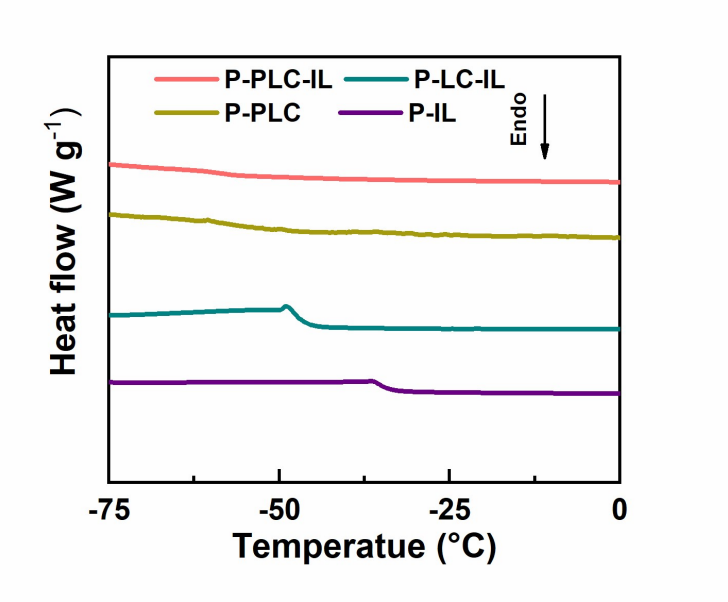

Fig. S5 DSC profiles of the P-PLC-IL, P-LC-IL, P-PLC and P-IL SPEs.

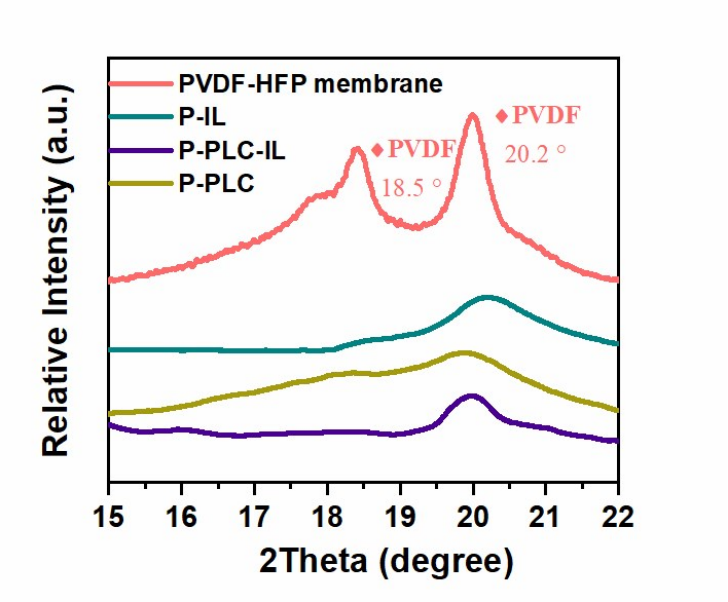

Fig. S6 XRD patterns of PVDF, P-IL, P-PLC and P-PLC-IL

For the pure PVDF-HFP samples, two strong diffraction peaks are observed at the 2θ value of 18.5 θ and 20.4 θ, which corresponds to the α-phase crystals and β-phase crystals of the PVDF-HFP phase[2], respectively. However, the two diffraction peaks were distinctively weakened in the P-PLC-IL samples, indicating that the α-phase and β-phase crystals were effectively suppressed in the P-PLC-IL[3].

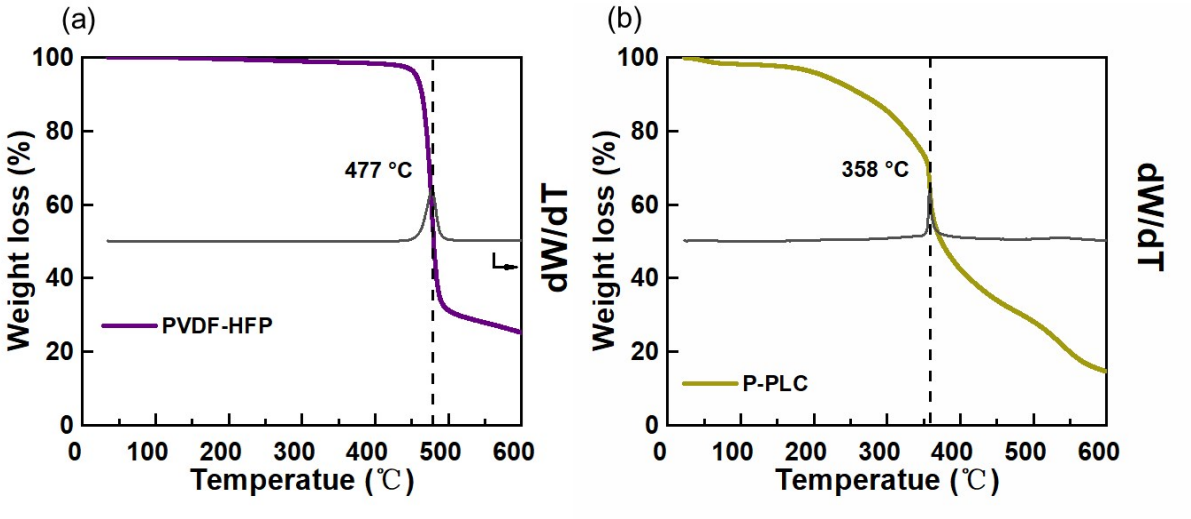

Fig. S7 TGA curves of (a) PVDF-HFP and (b) P-PLC

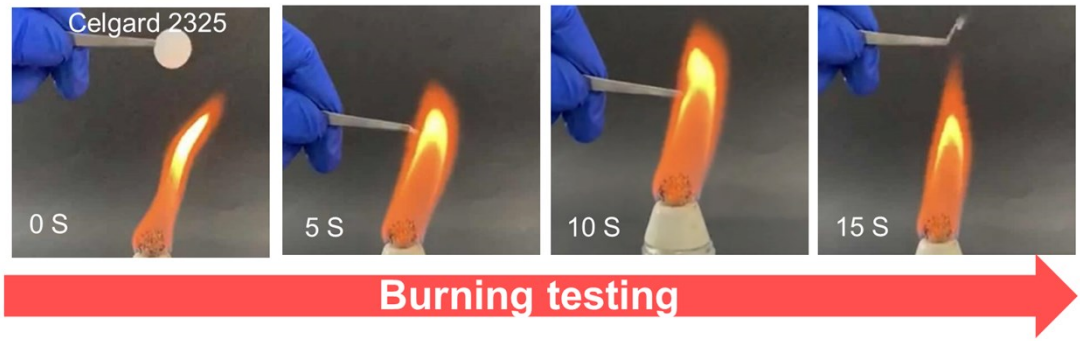

Fig. S8 Celgard 2325 with a fire from an alcohol lamp

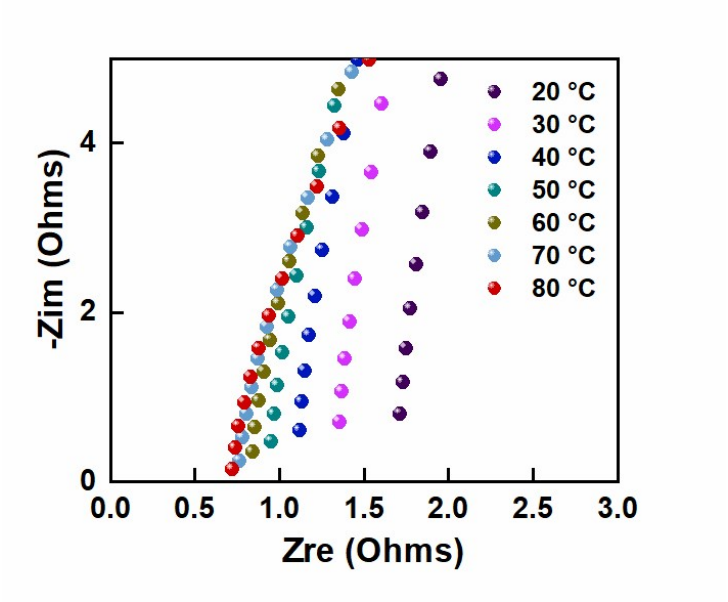

Fig. S9 Nyquist plots of SS/P-PLC-IL/SS at various temperatures

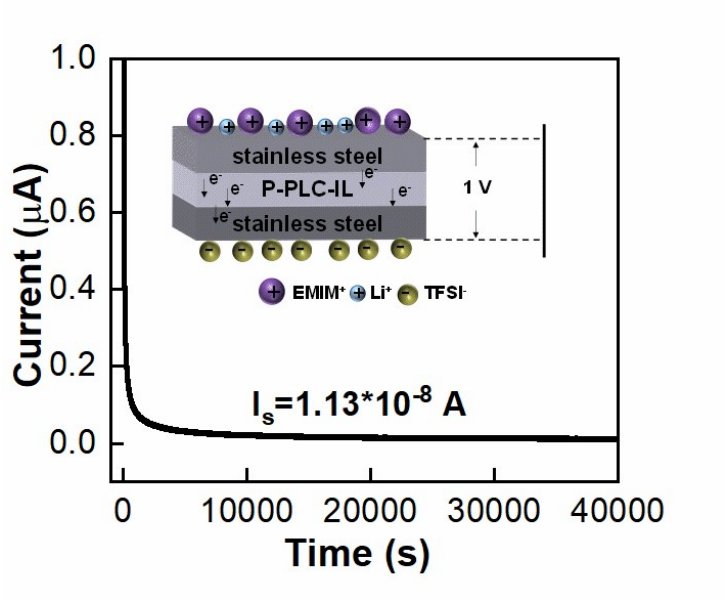

Fig. S10 Electronic conductivity of P-PLC-IL

Electronic conductivity was determined at room temperature using potentiostatic coulometry measurements, run on a symmetric SS/P-PLC-IL/SS cell and applying a 1 V polarization (U). Under given cell conditions, the ion flow decreased with time due to the pile-up of ions at the SS electrode. The electronic flow remained constant during the experiment as a result of the blocking effect of the electrodes

Sample	A (S cm^{-1}K$^{1/2}$)	T_0 (K)	E_a (kJ mol^{-1})	R^2
P-IL	0.48	237.1	2.50	0.982
P-PLC	0.12	208.3	1.43	0.991
P-LC-IL	0.75	224.4	2.59	0.991
P-PLC-IL	0.33	207.3	1.54	0.998

Tab. S1 The respective VTF parameters and results of P-IL, P-LC-IL, P-PLC and P-PLC-IL.

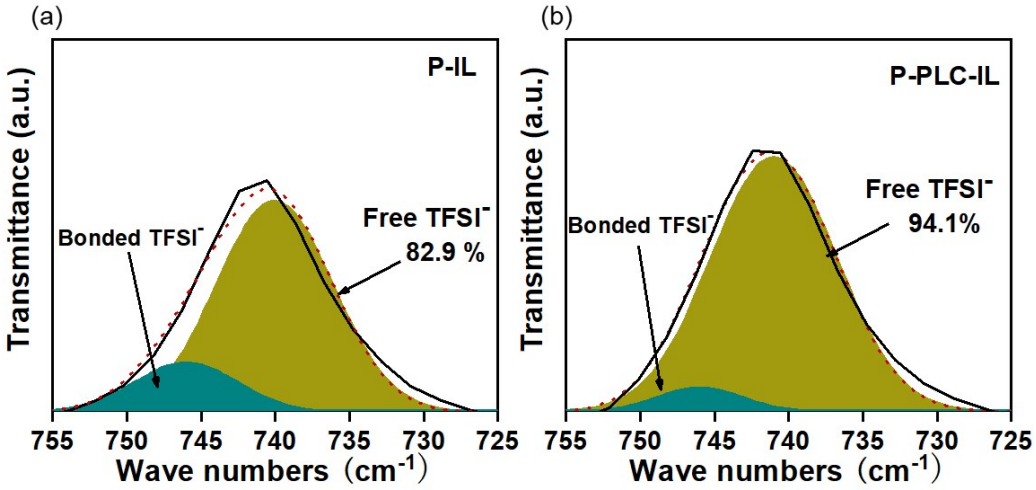

Fig. S11 FT-IR spectra with Gasussian-Lorentzian fitting curves of the (a) P-PLC-IL and (b) P-IL.

The FT-IR spectra with wavenumber ranging from 725 to 755 cm^{-1} are displayed to evaluate the dissociation degree of LiTFSI in P-PLC-IL and P-IL. The peaks at ~ 740 cm^{-1} and ~746 cm^{-1} can be assigned to the free $TFSI^-$ and bonded Li-TFSI ion pairs, respectively[4].

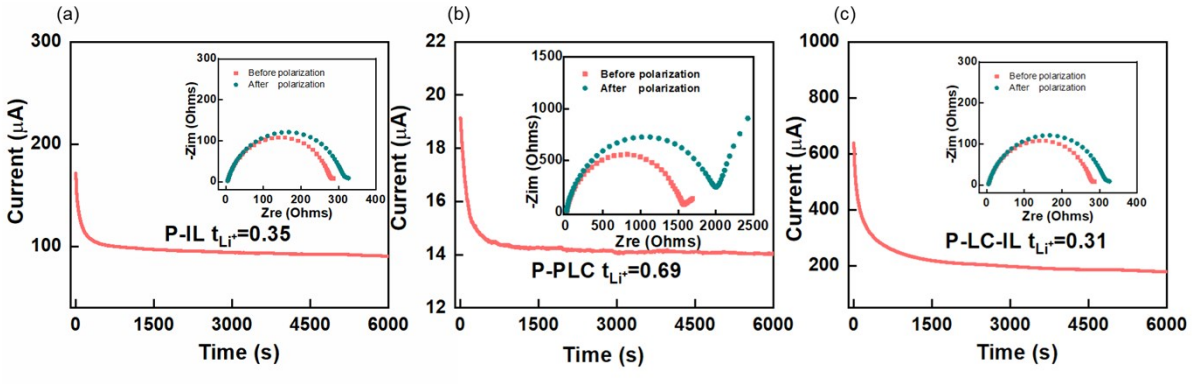

Fig. S12 a, b, c) The chronoamperometry profiles of symmetric Li/SPE/Li battery with potential steps of 50 mV at room temperature. Inset: the EIS before and after polarization.

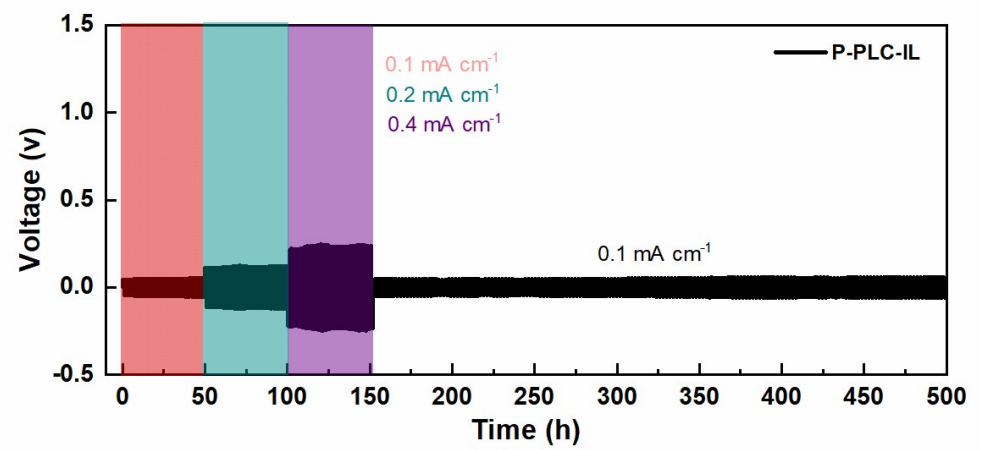

Fig. S13 Galvanostatic charge/discharge tests of lithium symmetric batteries assembled with P-PLC-IL at 0.1, 0.2 and 0.4 mA cm^{-2}

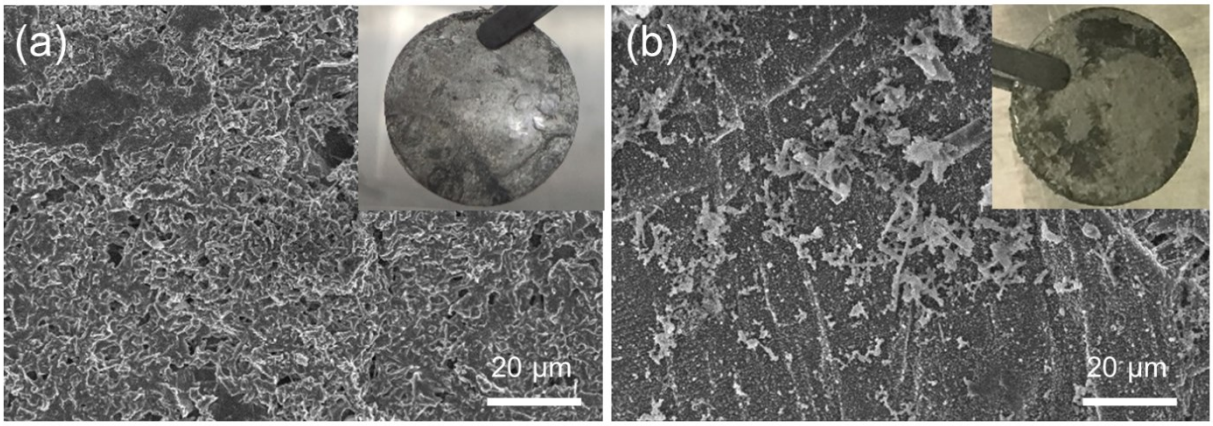

Fig. S14 a, b) surface SEM images of lithium chip from Li/P-LC-IL/Li and Li/P-PLC /Li after 100 h at 0.2 mA cm^{-2}

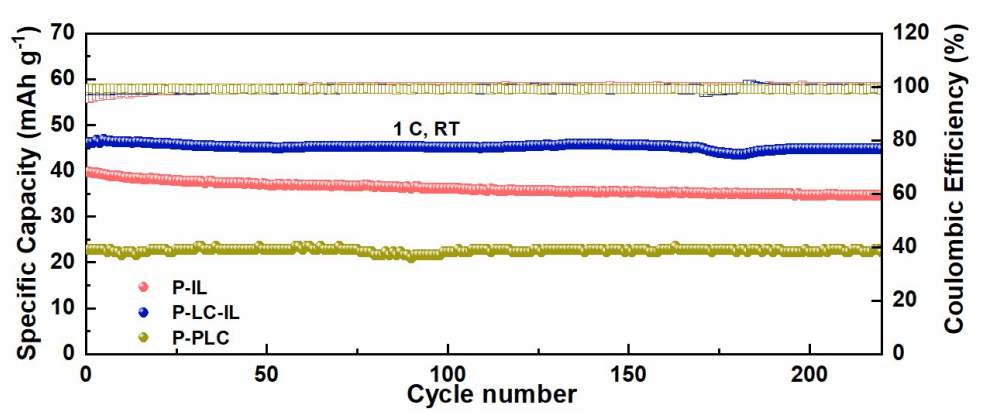

Fig. S15 Cycling performance of the P-IL, P-LC-IL and P-PLC based batteries under 1 C rate at room temperature

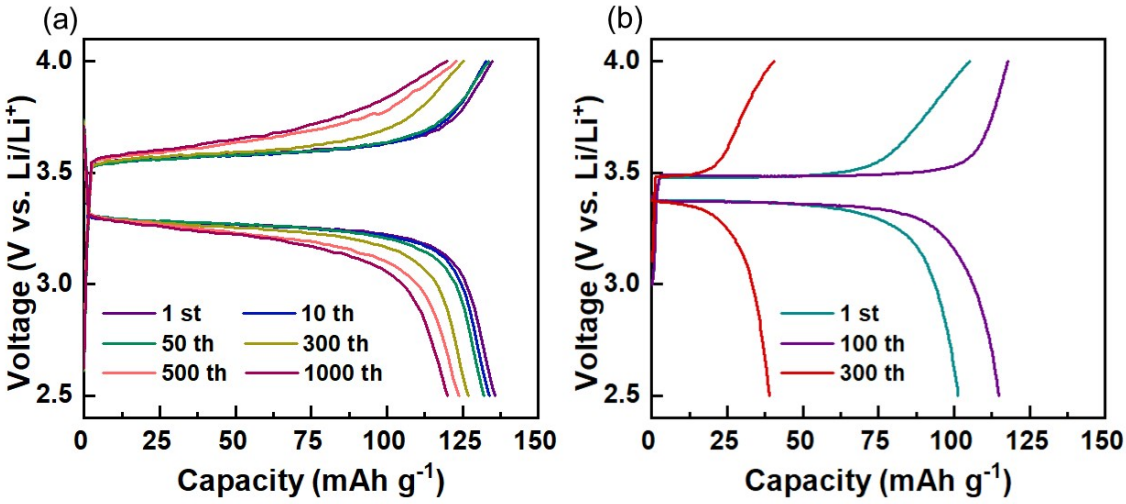

Fig. S16 Representative charge/discharge profiles of the (a) Li/P-PLC-IL/LFP and (b) Li/Celgard/LFP full cell at 1 C at room temperature

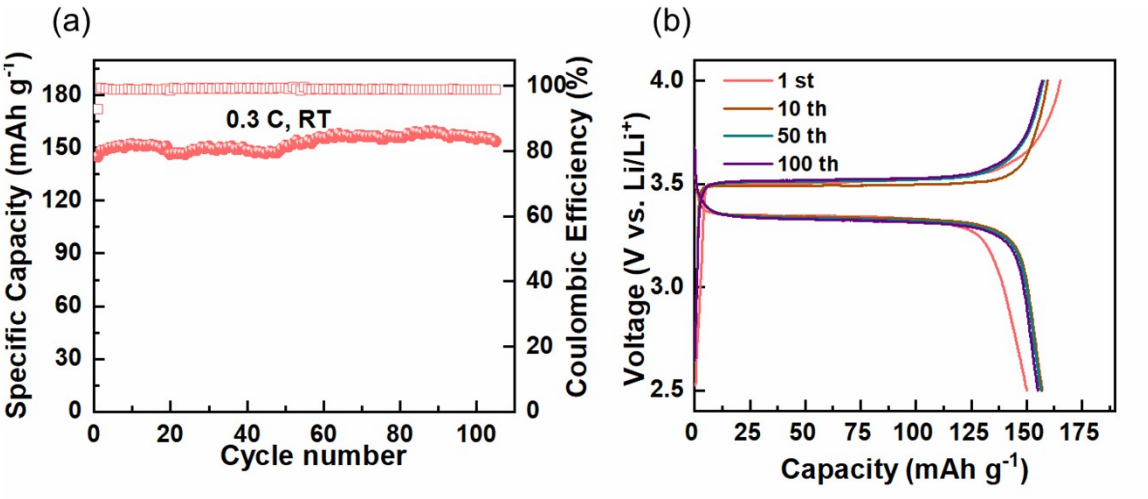

Fig. S17 a) The cycle performance of Li/P-PLC-IL/LFP full battery at 0.3 C at room temperature; b) representative charge/discharge profiles of Li/P-PLC-IL/LFP full battery

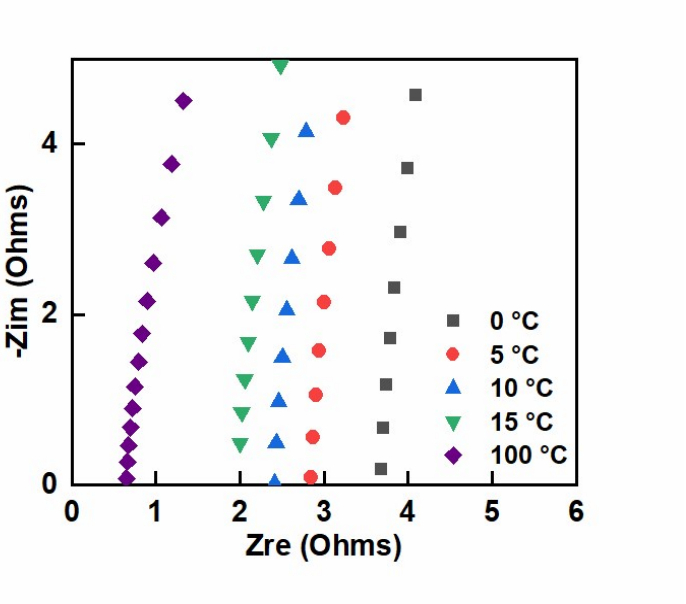

Fig. S18 Nyquist plots of the SS/P-PLC-IL/SS at various temperatures

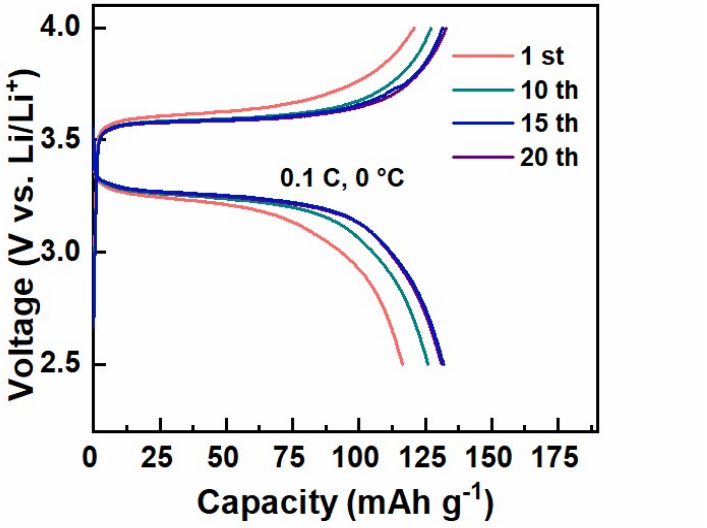

Fig. S19 Representative charge/discharge profiles of Li/P-PLC-IL/LFP full battery under 0.1 C rate at 0 °C

It should be noted that the overpotentials of cell decreased gradually in the initial 10 cycles, and remain unchanged in the following 10 cycles, indicating the improved ionic transport at the interface after cycles of activation.

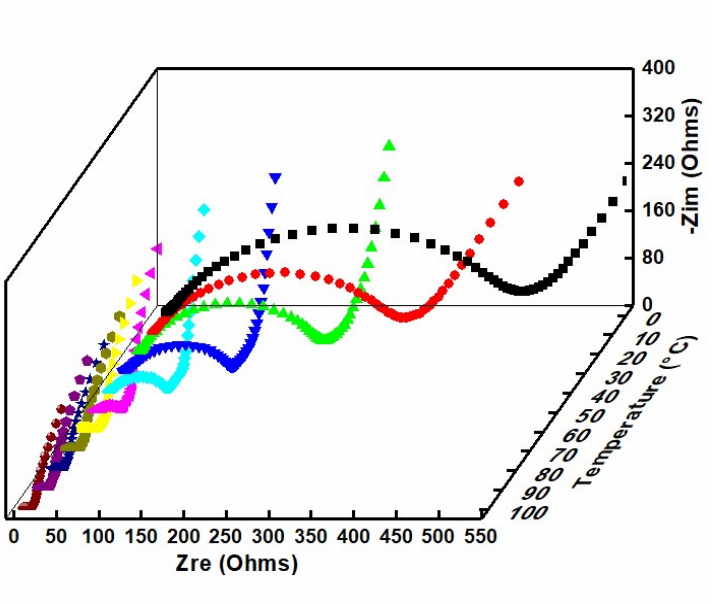

Fig. S20 Nyquist plots of the of fresh Li/P-PLC-IL/Li cell measured at various temperatures.

Reference	Membrane materials	conductivity at RT / mS cm-1	potential / V (vs.	Li symmteric cell performance	Capacity of Li/LiFePO4 battery / mAh g-1
[5]	UV cross-linked PEO/LiTFSI/Pyr_{14}TFSI	0.37 at 20 °C	5.0	> 2000 h (40 °C, 0.078 mA cm^{-2}, 1 h)	40 °C: 164 (0.1 C); ~140 (0.2 C); ~75 (0.5 C); ~60 (1 C); ~50 (2 C)
[6]	POSS/PEG/ LiFSI/Pyr_{13}FSI	0.60 at 20 °C	5.3	>130h (1 mA cm^{-2}, 1 h)	0 °C: 85 (0.1 C); 20 °C: 145 (0.1 C); 90 °C: 135 (1 C);
[7]	PDADMATFSI/P_{1118}DMP/LiFSI/Al_2O_3	0.28 at 30 °C	5.0	> 200 h (50 °C, 0.05 mA cm^{-2}, 1 h)	
[8]	PVDF/LLZTO/LiTFSI	0.24 at 20 °C	4.7	> 1000 h (20 °C, 0.05 mA cm^{-2}, 1 h)	20 °C: 142 (0.1 C); 98 (0.1 C)
[9]	PDADMATFSI/LiTFSI/Pyr_{14}TFSI	0.16 at 20 °C	5.0	> 4200 h (40 °C, 0.05 mA cm^{-2}, 1 h)	40 °C: 148.4 (0.05 C), 144.1 (0.1 C), 135.3 (0.2 C), 51.1 (0.5 C)
[10]	PDMA/Li(G4)TFSI/SiO_2	0.12 at 20 °C	4.5	> 400 h (20 °C, 0.05 mA cm^{-2}, 2 h)	55°C: 144 (1 C), 136 (2 C), 128 (3 C), and 110 (5 C)
[11]	UV cross-linked BC/LiTFSI/Pyr_{13}TFSI	0.24 at 25 °C	4.8		30 °C: 142.2 (0.1 C)
[12]	PAN/PEG/EPTEA/SiO_2/LiTFSI	0.89 at 25 °C	4.5	> 2000 h (20 °C, 0.5 mA cm^{-2}, 1 h with liquid electrolyte)	20 °C: 134 (0.5 C);
[13]	PEO/HPMA/LiTFSI	0.11 at 35 °C	5.3	> 1000 h (35 °C, 0.05 mA cm-2, 1 h)	35 °C: 162.6 (0.1 C); 149 (0.3 C); 135.9 (0.5 C)
This work	PVDF-HFP/PLC/EMIMTFSI/LiTFSI	1.79 at 20 °C	5.0	> 3 500 h (20 °C, 0.2 mA cm^{-2}, 1 h)	0 °C: 135 (0.1 C); 20 °C: 162.2 (0.1 C); 154.2 (0.3 C); 148.4 (0.5 C); 127.3 (1 C); 111 (3C); 100 °C: 165.9 (1 C); 163.2 (3 C); 158.8 (5 C)

Tab. S2. Comparison of our work with previously reported SPEs[5-13].

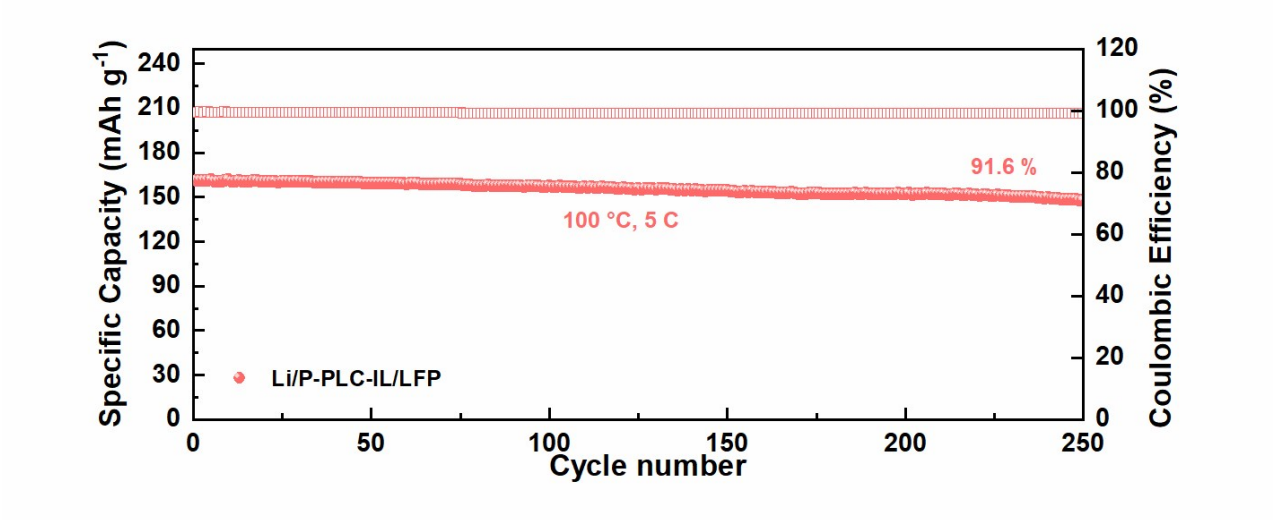

Fig. S21 The cycling performance of Li/P-PLC-IL/LFP under 5 C rate at 100 °C

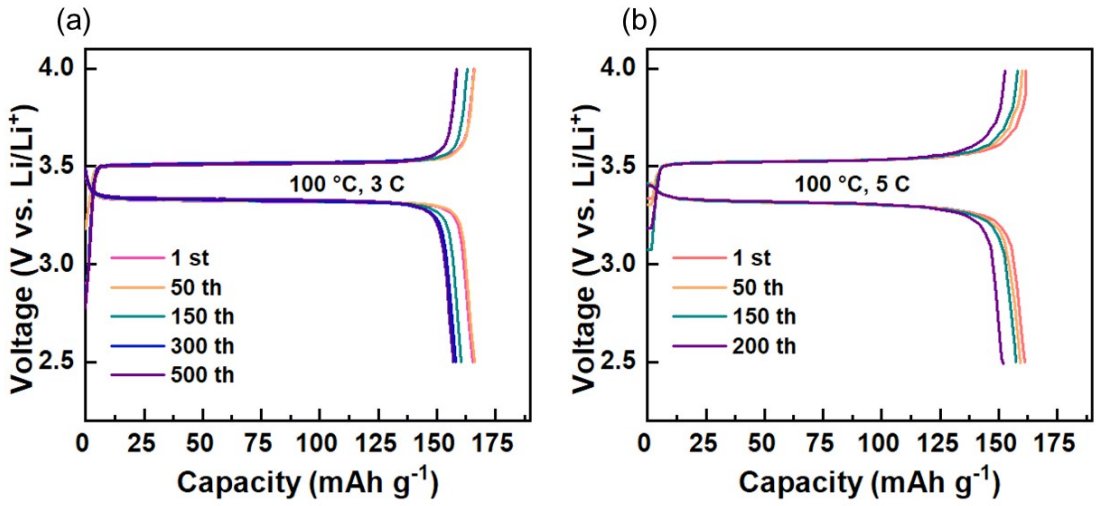

Fig. S22 Representative charge/discharge profiles of the Li/P-PLC-IL/LFP full battery under 3 C rate (a) and 5 C (b) rate at 100 °C

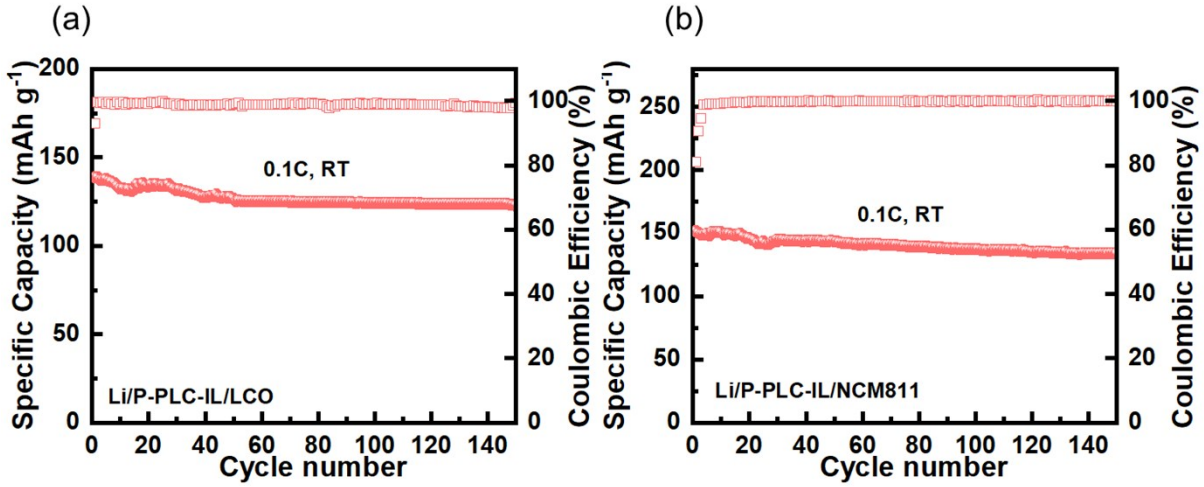

Fig. S23 a, b) Discharge capacity and Coulombic efficiency of Li/P-PLC-IL/LCO and Li/P-PLC-IL/NCM811 at room temperature under 0.1 C;

All of two battery delivered a relatively initial Coulombic efficiency (93 % to LCO, 81 % to NCM811), which may due to the formation of SEI film on the electrodes surface [14, 15].

References

[1] B. Park, J.L. Schaefer, J. Electrochem. Soc. 167 (2020) 070545.
[2] Y. Yang, Q. Wu, D. Wang, C. Ma, Z. Chen, C. Zhu, Y. Gao, C. Li, J. Membr. Sci. 595 (2020) 117549.
[3] Y. Yang, Q. Wu, D. Wang, C. Ma, Z. Chen, Q. Su, C. Zhu, C. Li, J. Membr. Sci. 612 (2020) 118424.
[4] X. Guan, Q. Wu, X. Zhang, X. Guo, C. Li, J. Xu, Chem. Eng. J. 382 (2020) 122935.
[5] G.T. Kim, G.B. Appetecchi, M. Carewska, M. Joost, A. Balducci, M. Winter, S. Passerini, J. Power Sources 195 (2010) 6130-6137.
[6] X. Li, Y. Zheng, C.Y. Li, Energy Storage Mater. 29 (2020) 273-280.
[7] X. Wang, H. Zhu, Gaetan M.A. Girard, R. Yunis, D.R. MacFarlane, D. Mecerreyes, A.J. Bhattacharyya, P.C. Howlett, M. Forsyth, J. Mater. Chem. A 5 (2017) 23844-23852.
[8] S. Zhang, Z. Li, Y. Guo, L. Cai, P. Manikandan, K. Zhao, Y. Li, V.G. Pol, Chem. Eng. J. 400 (2020) 125996.
[9] G.B. Appetecchi, G.T. Kim, M. Montanino, M. Carewska, R. Marcilla, D. Mecerreyes, I. De Meatza, J. Power Sources 195 (2010) 3668-3675.
[10] L. Yu, S. Guo, Y. Lu, Y. Li, X. Lan, D. Wu, R. Li, S. Wu, X. Hu, Adv. Energy Mater. 9 (2019) 1900257.
[11] M. Yan, W. Qu, Q. Su, S. Chen, Y. Xing, Y. Huang, N. Chen, Y. Li, L. Li, F. Wu, R. Chen, ACS Appl. Mater. Inter. 12 (2020) 13950-13958.
[12] W. Fan, X. Zhang, C. Li, S. Zhao, J. Wang, ACS Appl. Energy Mater. 2 (2019) 4513-4520.
[13] G. Wang, X. Zhu, A. Rashid, Z. Hu, P. Sun, Q. Zhang, L. Zhang, J. Mater. Chem. A 8 (2020) 13351-13363.
[14] A. Pelz, T.S. Dörr, P. Zhang, P.W. de Oliveira, M. Winter, H.-D. Wiemhöfer, T. Kraus, Chem. Mater. 31 (2019) 277-285.
[15] D. Lin, P.Y. Yuen, Y. Liu, W. Liu, N. Liu, R.H. Dauskardt, Y. Cui, Adv. Mater. 30 (2018) 1802661.